# Persistent Monitoring of Large Environments with Robot Deployment Scheduling in between Remote Sensing Cycles

Kizito Masaba, Monika Roznere, Mingi Jeong, and Alberto Quattrini Li

Abstract—This paper proposes a novel decision-making framework for planning "when" and "where" to deploy robots based on prior data with the goal of persistently monitoring a spatio-temporal phenomenon in an environment. We specifically focus on large lake monitoring, where remote sensors, such as satellites, can provide a snapshot of the target phenomenon at regular cycles. Between these cycles, Autonomous Surface Vehicles (ASVs) can be deployed to maintain an up-to-date model of the phenomenon. However, deploying ASVs has a significant logistical overhead in terms of time and cost. It requires a team of people to go on site and spend typically a day to monitor the deployment. It is vital to not only be intentional about where to sample in the environment on a given day, but also determine the worth of deploying the ASVs that day at all. Therefore, we propose a persistent monitoring strategy that provides the days and locations of when and where to sample with the robots by leveraging Gaussian Process model estimates of future trends based on collected remote sensing and point measurement data. Our approach minimizes the number of days and locations for sampling, while preserving the quality of estimates. Through simulation experiments using realistic spatio-temporal datasets, we demonstrate the benefits of our approach over traditional deployment strategies, including significant savings on the effort and operational cost of deploying the ASVs.

## I. Introduction

We present a novel decision-making approach for planning "when" and "where" to deploy robots to sample, based on remote sensing data, to efficiently and accurately reconstruct a spatio-temporal phenomenon over a long-time horizon. The remote sensing data of the full environment is provided at fixed known intervals, while the robots sample smaller regions of interest during the remote sensing interludes. See Fig. 1 for a depiction of the problem.

Monitoring spatio-temporal phenomena is important for a number of high-impact applications, including environmental monitoring and precision agriculture [1]. A common sensing modality for such applications is hyperspectral imagery from various satellites [2]. While satellite flyovers occur at regular known intervals, the periods between data acquisition is somewhat large, e.g., LandSat's flyovers occur every two weeks. In order to persistently monitor a phenomenon of interest in the environment, it is crucial to utilize other data-collection technologies. For instance, water quality monitoring has been carried out with water quality measuring sondes carried by Autonomous Surface Vehicles (ASVs) [3]–[5] and

The authors are in the Department of Computer Science, Dartmouth College, Hanover, NH, USA, 03755 {kizito.masaba.gr, monika.roznere.gr, mingi.jeong.gr, alberto.quattrini.li} @dartmouth.edu

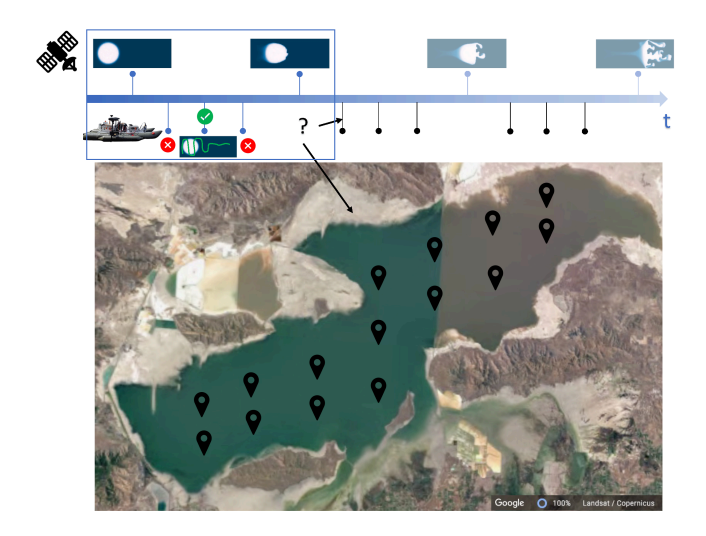


Fig. 1. Scenario: Given a region of interest with a spatio-temporal field, F, for which remote sensing data is available at regular intervals, and a robot, R (equipped with a sensor that can measure the field), which needs to coordinate with the remote sensor in order to persistently monitor F over a long period. On "which days" and at "which locations" should R be deployed so that the uncertainty of the estimated spatial field remains low and the cost of operating R is minimized?

images captured by a downward facing camera mounted on Unmanned Aerial Vehicles (UAVs) [6].

Most current research pursues strategies using robots to cover and sample regions of interest for one day's purpose [7]. However, many real-world phenomena in environments need to be monitored over long periods of time. Therefore, multiple robotic deployments are typically required over a 'season' of monitoring. Moreover, there is high logistical cost and overhead for deployments, such as traveling to the site, coordinating with team members, and ensuring the robot safety. Thus, it is generally difficult to conduct daily sampling campaigns.

Our goals are to reduce the on-site sampling burden and be more intentional on how the robotic deployment is conducted. We propose a strategy that exploits prior data, from both the remotely sensed and on-site sampled data, to decide whether a robot sampling deployment is necessary on a given day and, if so, where the robot(s) should sample – all of which to ensure an accurate daily estimate of the target spatio-temporal phenomena.

In particular, the main contributions include:

A modeling framework based on a Mixture of Gaussian Process Experts (MoGPE) approach to quantify
the uncertainty over time from the accumulated data,
consisting of data from remote sensors and previous

robotic deployments.

- A novel decision-making framework, based on the aforementioned modeling framework, for spatiotemporal sampling over a long-time horizon.
- Analysis of the tradeoff between efficiency and accuracy

   i.e., minimizing or maximizing the number of sampling performed through experiments on synthetic and real-world phenomena.

Experimental results demonstrate that our method significantly reduces the number of sampling days while also preserving the quality of model reconstruction. This work represents the foundation of long-term spatio-temporal sampling to support scientists in their endeavor to monitor and protect our environment.

The paper is structured as follows. The next section discusses related work specifically focusing on spatio-temporal monitoring. Section III formally states the sampling problem of focus. Section IV describes the modeling used for keeping track of changes in the uncertainty over time, which allows for decisions to be taken on when and where to sample, as presented in Section V. Experimental setup, results and concluding remarks are presented in Section VI, VII, and VIII respectively.

## II. RELATED WORK

Several approaches have been proposed for sampling in a region of interest, where robots have to collect spatial information in the environment. Such approaches typically fall in two categories, *coverage* [8]–[10] with robots that have to cover every point in the region of interest with the sensor footprint; and *adaptive sampling* [11]–[14] where robots will adapt to measurements taken during the mission. Some recent surveys on exploration and sampling include [7], [15]. The mainstream methods look at spatial sampling in static environments, neglecting the temporal components important in expeditionary science [16]. Here, we highlight the work that focuses on spatio-temporal monitoring.

Spatio-temporal monitoring can be achieved by having robots following preplanned missions [17] or offline optimized paths [18] and collecting data repeatedly. Some adaptation of preplanned missions to external factors can allow persistent monitoring in the ocean [19]. Reactive strategies like artificial potential field can also be found in the literature [20]. Graphs can represent the locations and their connections that the robots need to visit; when the objective function is submodular, i.e., when a sample from a location provides less utility because other closer locations have already been sampled, a greedy algorithm can have approximation guarantees [21]. Gaussian Processes (GPs) have been used for modeling the spatio-temporal map, where for example the robot moves following a simple behavior [22]. More commonly, GPs are used for finding paths that maximize the information gain and minimize the traveled distance [23]-[25]. Monte Carlo Tree Search (MCTS) is another technique used to balance exploration and exploitation and is shown to capture time dynamics [26], [27]. [28] compared in simulation a number of different methods for

sampling in ocean areas above a certain threshold ranging from boustrophedon [8] to sequential Bayesian optimization [29]. The latter, an adaptive sampling method, outperforms the others. Some methods model explicitly dynamics so that the exploration strategy can predict environment change and accordingly decide when to explore a specific area [30]. In a multi-robot scenario, some work have looked at distributing the workload fairly by geometrically subdividing the region of interest [31]. A distributed multi-robot strategy exploits a reduced-order model from sparse measurements in order to then estimate areas without measurements and accordingly reconfigure the sensing locations [32].

There have also been attempts on combining different sensor streams and proposing sampling strategies, such as mobile robots and static nodes [33], ASV with UAV [34], [35] and ASV with satellite [36]. Their goal was to enhance the efficiency of the sampling mission by compensating the weakness of one sensor stream and leveraging the strength of another sensor stream.

Differently from the current literature, our objective is to use prior data to take informed decisions on days when to deploy the robots and sample rather than making arbitrary deployments.

## III. PROBLEM STATEMENT

Our aim is to estimate the state of an unknown spatiotemporal phenomenon F in a 2D environment  $\mathscr{E} \subset \mathbb{R}^2$ , during a monitoring period with a long-time horizon T. Specifically,  $F = \bigcup_{t=1}^T F_t$ , where  $F_t$  is a snapshot of F at some time step t.

We utilize two heterogeneous sensors,  $Z_S$  and  $Z_G$  that observe F at comparable spatial resolutions.  $Z_S$  is a remote sensing tool (e.g., satellite) that observes  $F_t$  at fixed time intervals  $T_S$ , where  $1 < T_S \le T$ , to obtain the data  $D_S = \{D_{iT_S}\}, \forall i \in \{0, \dots, \frac{T}{T_S}\}$ .  $Z_G$  is a point measurement sensor (e.g., ASV) that can observe  $F_{t_D}$  if deployed at  $t_D$  to obtain the data  $D_G = \{D_{t_D}\}$ . Note that  $t_D$  is unknown, as it represents the time steps of when to deploy  $Z_G$ .

We assume  $D_S$  and  $D_G$  can be transformed into a common space Z by some function  $\Psi: D_* \mapsto Z$ , such that  $F_t = f(\Psi(D_*)) + \varepsilon$ , where  $\varepsilon \sim \mathcal{N}(0, \sigma^2)$  is the Gaussian noise in  $\Psi(D_*)$ . Given  $\Psi$ ,  $Z_S$  and  $Z_G$  do not need to collect data during the same time step. Since  $Z_S$ 's time schedule is known and set, only  $Z_G$ 's schedule needs to be optimized, by minimizing the cost of deployment and operation while preserving a predictive accuracy,  $\Delta$  of  $F_t$ .

Thus, our goals are:

- 1) To determine the time  $t_D$  in the future of when to deploy  $Z_G$  while preserving the desired predictive accuracy, and
- 2) Given  $t_D$ , to identify the critical locations  $X_c$  that  $Z_G$  must sample.

# IV. SPATIO-TEMPORAL FIELD MODELLING

As our proposed approach is based on GPs and their properties, here we include a brief description of the GPs together with an analysis on the accuracy of the estimates.

Let D = [X,Y] be a dataset, where X is a 3D vector with  $(t,p,q) \in X$ , with  $t \in \mathbb{R}$  being time and  $(p,q) \in \mathscr{E}$  a location in  $\mathscr{E}$ . Let Y be a vector of their corresponding measurements,  $y = \Psi(D_*) + \varepsilon$  collected by any given sensor, such that for every  $(t,p,q) \in X$ , there is a corresponding  $y \in Y$ . Let  $X_*$  be a 3D vector of test inputs, whose corresponding measurements,  $Y_*$  are to be estimated. Then, a GP model  $f_*$  for estimating  $X_*$  is drawn from a normal distribution defined as

$$f_*|X,Y,X_* \sim \mathcal{N}(\mu(X,X_*),\Sigma),\tag{1}$$

where the mean vector  $\mu(X, X_*)$  and covariance matrix  $\Sigma$  are

$$\mu(X, X_*) = K(X_*, X)[K(X, X) + \sigma_n^2 I]^{-1}Y, \tag{2}$$

$$\Sigma = K(X_*, X_*) - K(X_*, X)[K(X, X) + \sigma_n^2 I]^{-1} K(X, X_*).$$
 (3)

The elements of the covariance matrix,  $K(\cdot,\cdot)$  are given by a kernel function, which describes the spatio-temporal correlation between a pair of inputs. We apply a commonly used kernel because of its general applicability to different domains, the squared exponential (SE), [37], defined as

$$k_y(x_p, x_q) = \sigma_f^2 \exp(-\frac{(x_p - x_q)^2}{2l^2}) + \sigma_n^2 \sigma_{pq},$$
 (4)

where l is the length scale representing the function smoothness;  $\sigma_f^2$  is signal variance determining the amplitude;  $\sigma_n^2$  is the noise variance accounting for the estimate noise; and  $\delta_{pq}$  is the Kronecker delta ( $\delta_{pq}=1$  if p=q, else  $\delta_{pq}=0$ ).

Using the SE kernel, a GP model is parameterized by  $\theta = (\sigma_f^2, l, \sigma_n^2)$ , which are determined from the data using Maximum Likelihood Estimation (MLE) [37], by maximizing

$$\log p(Y|X,\theta) = -\frac{1}{2}Y^{T}\Sigma_{y}^{-1}Y - \frac{1}{2}\log|\Sigma_{y}| - \frac{n}{2}\log 2\pi. \quad (5)$$

Assuming we are given an accurate GPR estimator,  $\hat{\theta}$  that estimates some random variable  $\theta$ ; the Mean Squared Error (MSE) [38] in the estimates is given by

$$MSE(\hat{\theta}) = E[(\hat{\theta} - \theta)^2]. \tag{6}$$

We can express  $E[(\hat{\theta} - \theta)^2]$  in terms of the GPR variance to obtain [38]

$$MSE(\hat{\theta}) = Var(\hat{\theta}) + Bias^{2}(\hat{\theta}). \tag{7}$$

where  $Var(\hat{\theta})$  is the posterior variance of GPR and  $Bias(\hat{\theta})$  is the model bias. Accordingly, for an unbiased estimator as a GP [39]

$$Var(\hat{\theta}) \le MSE(\hat{\theta}) = \Delta,$$
 (8)

where  $\Delta$  is a MSE constant that can be predefined by the user. From Equation (8), we can define the accuracy of GPR estimates as a function of its posterior variance. Based on this formulation, we define a desired accuracy value,  $\Delta$ , to determine the efficiency of the adaptive sampling mission.

Note that the running time and memory complexity of GP modeling is  $O(N^3)$  and  $O(N^2)$ , respectively [37] – where N is the size of the training set D. This makes the GP model intractable for real-time exploration of large areas (e.g., N > 100 on an embedded system). We'll show in the next section how we address this challenge.

#### V. SENSOR SCHEDULING ALGORITHM

Suppose we have a time series of snapshots of a spatiotemporal field. Then, its future flow can be predicted using various models [37], [40], one of which is a Gaussian Process Regression (GPR) model just described. In this section, we describe how a GPR can be used to optimize the schedule of sensors utilized in a persistent monitoring task.

Initially, we need to strategically identify *hot-spot lo-cations*,  $X \in \mathcal{E}$ , whose measurements at any given time t are sufficient for reconstructing the snapshot  $F_t \subset F$  of the field. The goal is to minimize the number of data points required for modeling F and the cost of operating sensor  $Z_G$ , while also preserving the predictive accuracy of the estimates. One strategy for determining hot spots is to divide the environment into cells of a particular resolution and use the measurements from the center of each cell in the modeling. Note, the resolution can be empirically optimized for a given predictive accuracy  $\Delta$ , using a GPR model.

Assuming the historical measurements of F, specifically  $D_t = \bigcup_{i=-\infty}^t D_i$  taken up to t from X, can be used to accurately reconstruct  $F_t$ , the following properties are upheld:

- 1) Spatial variability:  $D_t$  captures the spatial variations (non-stationarity) that occurs in  $F_t, \forall t = 1, ..., T$ .
- 2) Temporal variability:  $D_t$  captures the temporal variations in F that occurs within the time window  $[-\infty, t]$ .

With the *spatial variability* property, the task of monitoring spatial variations in  $F_t$  can be reduced to monitoring *hot-spot locations* X at t. This minimizes the computational cost of modeling  $F_t$  and the operational cost of sampling with sensor  $Z_G$ . On the other hand, the *temporal variability* property allows us to predict temporal variations that may occur at every location  $x \in X$  and, hence, identify those that may require sampling in the near future for proper planning. We leverage these properties in designing the proposed approach for scheduling the deployment of the on-demand sensor  $Z_G$ .

# A. Predicting Future States

Given X,  $D_t$  (i.e., all data collected up to t,) and a desired predictive accuracy  $\Delta$ , our goal is to predict snapshots  $F_{T_c} = \{F_i, \forall i = t, t+1, \ldots, t+T_c\}$  for timestamped *hotspot* locations  $X_{T_c}$ , where  $T_c$  is the remaining number of time steps from t to the end of the current cycle for sensor  $Z_S$ . We focus on this particular time window because no new data is collected from any sensor in this period, making it the right time to decide on whether or not to deploy  $Z_G$ . To obtain  $F_{T_c}$ , we can train a GPR model with  $D_t$  and use it for prediction. However due to the high computational demands of GPR, this approach may become intractable as the size of  $D_t$  increases over time. To address this, we propose a mixture of GP experts approach outlined in Algorithm 1.

In this approach,  $D_t$  is partitioned into clusters and each cluster is used to train a GPR model that makes local predictions of  $X_{T_c}$ , denoted as  $\hat{Y}_c$  (lines 2-6). We assume that the resulting clusters categorize  $D_t$  into i.i.d. subsets that can be modeled by a GPR, and the trained GPR can estimate new

## **Algorithm 1** Predict Future States, $F_{T_c}$

```
Input: t, D, X_{T_c}, T; Time step, Prior Data up to t, Timestamped hot spot
locations, Time horizon
Output: \mu_{Y_c}, \Sigma_{T_c}; Estimates for X_t
  1: C, C_D, \leftarrow clusterData(D); Cluster ids, Clustered data
  2: \hat{Y}, \leftarrow {}; Cluster model estimates for X_t
  3: for all c \in C do
            \hat{Y}_c \leftarrow Predict(C_D[c], X_{T_c})
            \hat{Y}[c] \leftarrow \hat{Y_c}
  6: end for
 7: \mu_{T_c}, \Sigma_{T_c}, \leftarrow \emptyset, \emptyset
8: for all x_{i_{\underline{c}}} \in X_{T_c} do
            \mu_{x_i}, \sigma_{x_i}^2 \leftarrow \arg\min_{\hat{Y}_c^{x_i}} \{ \sigma_{x_i}^2 \in \hat{Y}_c^{x_i}, \forall c \in C \}
  9:
10:
            Add \mu_{x_i} to \mu_{T_c}
Add \sigma_{x_i}^2 to \Sigma_{T_c}
11:
12: end for
13: return \mu_{T_c}, \Sigma_{T_c}
```

inputs that are within its cluster. Hence, training a local GPR model for each cluster allows for finding optimal parameters that are representative of each cluster. We use the DBSCAN [41], [42] technique for clustering because of its superior performance on dynamic data [43] and its ability to optimize the number of clusters. Hence, we predict  $F_{T_c}$  by finding the most optimal estimate  $\hat{Y}_c^{x_i} \in Y_c$  for each instance  $x_i \in X_{T_c}$  among all of its local estimates, such that

$$F_{T_c} = \bigcup_{\forall x_i \in X_{T_c}} \hat{Y}_c^{x_i}. \tag{9}$$

We assume that the most optimal estimate is one with the smallest predictive accuracy (line 9). Note that  $F_{T_c}$  has two components: the posterior mean,  $\mu_{T_c}$ , and variance,  $\Sigma_{T_c}$ . We obtain the snapshot  $F_t$  from  $\mu_{T_c}$  and exploit  $\Sigma_{T_c}$  to determine the next *critical time t<sub>D</sub>* as well as the corresponding *critical locations X<sub>c</sub>* for scheduling  $Z_G$ , as described in the next section.

# B. Scheduling Next Deployment

At any given time t we can compute the *critical time*  $t_D$  and *critical locations*  $X_c$  by analyzing  $\Sigma_{T_c}$ , obtained from the model as described in Section V-A. Let snapshot  $\Sigma_c^{t_D} \subseteq \Sigma_{T_c}$  be the predictive accuracy for input  $X_{t_D} \subseteq X_{T_c}$  (i.e., X at time step  $t_D$ ). We consider  $\Sigma_c^{t_D}$  to be critical if its maximum value exceeds  $\Delta$  and if  $t_D$  is the closest time step to t. We refer critical time as  $t_D$ , where  $t_D > t$ , and critical locations as  $X_c \subseteq X_{t_D}$ , corresponding to values that exceed  $\Delta$ . (See Algorithm 2, line 15).

We demonstrate the application of the proposed algorithm with a toy example shown in Fig. 2. In this example, X contains 3 unique locations, P0, P1 and P2. The spatiotemporal field F exhibits unique variations at each location, such that the variation at P0, P1 and P2 are defined by linear functions  $f(t) = 6 + \varepsilon$ ,  $f(t) = 0.2t + 5 + \varepsilon$  and  $f(t) = 0.3t + 8 + \varepsilon$ , respectively, where  $\varepsilon \sim \mathcal{N}(0, \sigma^2)$  is Gaussian noise. In this example, we define  $F = \{f(t)\}, \forall t = 1, \dots, T = 50 \text{ (days)}$ . The goal is to predict the appropriate time for taking new samples, such that a desired predictive accuracy is maintained. Using data from Day 0-3  $(D_3)$  and from Day 0-10  $(D_{10})$ , collected by both sensors  $Z_S$  and  $Z_G$ , we

## Algorithm 2 Sensor scheduling Algorithm

```
Input: X,T,T_S; Hotspot locations, Time horizon, Sampling cycle of sensor
Output: F = \{F_t, \forall t = 1, ..., T\}; Daily estimates of F across T
 1: S,D,t,t_D \leftarrow \{\},\{\},0,-1; locations scheduled for sampling, collected
     sensor data, time step, predicted time step for deployment of sensor Z_G
     F \leftarrow \emptyset; Estimated Snapshots of F
     while t < T do
         S[t+1] \leftarrow \emptyset
 5:
         if t\%T_S = 0 or t = t_D then
             if t\%T_S = 0 then
 7:
                 D_S \leftarrow fetch data with sensor Z_S
 8:
                 D[t] \leftarrow \Psi(D_S)
 9:
10:
                 D_G \leftarrow Deploy sensor Z_G to sample at locations S[t_D]
                 D[t] \leftarrow \Psi(D_G)
11:
12:
13:
             X_{T_c} \leftarrow \text{generate timestamped } X \text{ from } t \text{ to } t + T_c
14:
             \mu_{T_c}, \Sigma_{T_c} \leftarrow predictFutureStates(t, D_t, X_{T_c}, T)
15:
             t_D, X_c \leftarrow scheduleNextDeployment(t, \Sigma_{T_c}, X, T_S)
16:
             S[t_D] \leftarrow X_c
             F_t \leftarrow \text{Extract estimates of } X_t \text{ from } \mu_{T_c}
17:
18:
19:
             F_t \leftarrow \text{Compute Estimate for } X_t \text{ from } D_t
20:
         end if
21:
         Add F_t to F
         t \leftarrow t + 1
23: end while
24: return
```

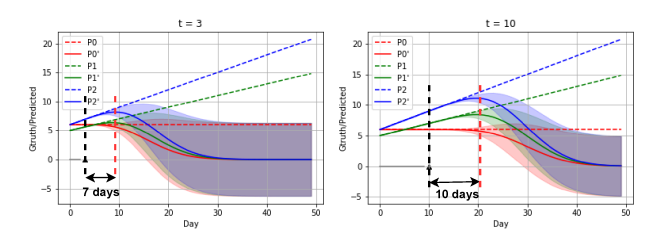


Fig. 2. GPR estimates for locations P0, P1, and P2, where their measurements are defined by functions  $f(t) = 6 + \varepsilon$ ,  $f(t) = 0.2t + 5 + \varepsilon$ , and  $f(t) = 0.3t + 8 + \varepsilon$ , respectively. Left: GPR Estimates after training the model with historical data up to day 3. The model accurately estimates the field up to 7 days in the future without requiring more samples. Right: GPR estimates after training the model with historical data up to day 10. The model accurately estimates the field up to 10 days in the future without requiring more samples.

train GPR models and then predict the progression of F in subsequent time-steps. With  $D_3$ , we observe that the model can accurately predict  $F_t$  for 7 consecutive days in the future without new samples of F. Similarly, we observe that  $D_{10}$  can accurately predict up to 10 consecutive days without new data. Consequently in both scenarios, sampling is only necessary at Day 10 and Day 20 respectively. Hence, we can deploy  $Z_G$  at these time steps (i.e., *critical time*) to locations  $X_c \subseteq X_{t_D}$  that need sampling (i.e., *critical locations*).

Note that if  $Z_S$  is scheduled within the 7-day or 10-day period, then deployment of  $Z_G$  is unnecessary, as an update of the model with new data from  $Z_S$  may extend the accurate prediction further out into the future. Hence, we optimize the deployment schedule of  $Z_G$  ( $t_D$  and  $X_{t_D}$ ) by iteratively optimizing the predictive accuracy bound of the GPR model whenever new data is introduced. On deployment,  $Z_G$  samples *critical locations* using an off-the-shelf path planner,

such as boustrophedon [8] or TSP [44].

## VI. EXPERIMENTS

We implemented the proposed approach in simulation and evaluated it using two unique spatio-temporal field datasets, *SF1* and *SF2*. Each dataset is a 100-frame video, where *SF1* simulates a realistic spread of a barium cloud and *SF2* simulates variation of water temperature over time. We obtained *SF1* from [35] and generated *SF2* synthetically with GSTOOLS [45]. We assume each video frame shows an accurate distribution of the field for a day, resulting in 100 days of ground truth data. Some snapshots from *SF1* and *SF2* are shown in Fig. 3. Both *SF1* and *SF2* are in a 400 m x 150 m environment with 200 hot-spot locations *X*, distributed at a resolution of 20 m.

Furthermore, we assume the remote sensor  $Z_S$  can accurately measure both SF1 and SF2 at fixed cycles  $T_S$  (in days). Whereas,  $Z_G$  can take in-situ measurements for both fields whenever it is deployed. We test different remote sensing cycles, 2, 5 and 10. For simplicity, we define  $\Psi(z) = z + \varepsilon$ , where z is a ground truth measurement and  $\varepsilon$  is Gaussian noise with 0 mean and variance, equivalent to 5% of the max value of the corresponding spatio-temporal field.

Our goal is to obtain accurate daily estimates of SF1 and SF2 at the hot-spot locations, while minimizing the number of deployments and visited locations,  $X_c \subseteq X$  of  $Z_G$ , throughout the 100-day period.

To achieve this, we consider four persistent monitoring strategies: 1) and 2) the proposed strategy is where  $Z_G$  is deployed to collect samples when necessary, and estimates are made based on both the collected data and the latest remote sensing data. This approach is further evaluated based on the adaptability of sampled locations when  $Z_G$  is deployed. We denote the approach where all locations are sampled at every deployment as ADAPT\_S and the approach where only critical hot-spot locations are sampled as ADAPT\_D. 3) The DAILY strategy is where  $Z_G$  is deployed daily (except on the days when  $Z_S$  is used) to collect samples, and estimates are made based on both the collected data and the latest remote sensing data. 4) The *REMOTE* strategy is where  $Z_G$  is never deployed, but estimates are made based on the previously collected remote sensing data. For all strategies, a GPR model described in Section IV provides the estimates based on the collected data.

Experiments were performed as a cron job on a Ubuntu machine with an Intel i7 CPU and 32GB RAM. For every deployment scheduled by the cron job, we spawned a team of four differential drive robots in Stage [46] simulator to traverse all hotspot locations scheduled for sampling. On deployment, we used the m Traveling Sales person (mTSP) [47] method, where m=4, to compute subtours for each robot. However, other path planning methods can be implemented. In addition, we limited prior data used in training the model to a window of 10 days for computational tractability purposes.

For evaluation, we report the root mean square error (RMSE) of the daily estimates made by each strategy, the

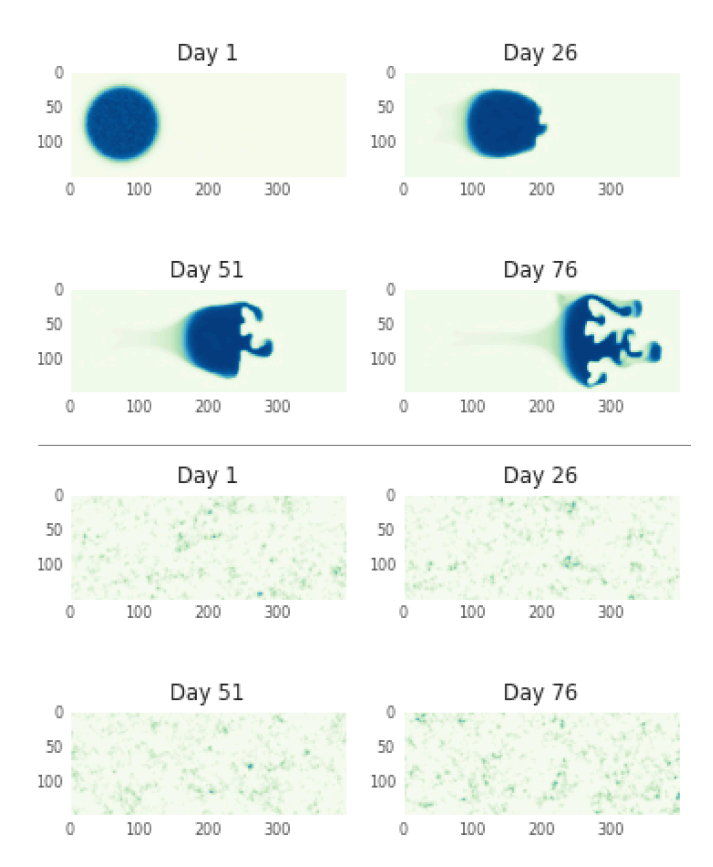


Fig. 3. Snapshots of the spatio-temporal fields, *SF1* (top) and *SF2* (bottom). *SF1* represents a barium cloud flow field, where a mass flows from the left to the right, while dispersing over time. *SF2* represents the variation of water temperature over time.

percentage of days  $Z_G$  is deployed across the entire monitoring duration, and the percentage of locations visited during each deployment. These metrics indicate the efficiency of persistent monitoring and the cost of operating  $Z_G$ .

In summary, we have two spatio-temporal fields, SF1 and SF2, and we would like to monitor them using sensor  $Z_S$  and  $Z_G$ .  $Z_S$  samples the fields every 2, 5, and 10 days, whereas  $Z_S$  is deployed using three different strategies:  $ADAPT\_S$ ,  $ADAPT\_D$ , and DAILY. In the next section, we evaluate the performance of the monitoring task, evaluating our methods against the alternative strategies.

## VII. RESULTS AND DISCUSSION

We observe that *DAILY* outperforms *ADAPT*\_\* and *RE-MOTE* throughout the entire monitoring period, for both *SF1* and *SF2* as shown in Fig. 4. This is due to *DAILY*'s ability to collect daily data, which improves accuracy in all its estimates. However, *ADAPT\_S* and *ADAPT\_D* follow closely in performance since, unlike, *DAILY*, they collect data only when it is deemed necessary. The *REMOTE* strategy has the highest *daily error* due to its reliance on only remote sensing data.

Fig. 5 reports the number of days on which  $Z_G$  is deployed as a percentage of days within the monitoring period. We note that *DAILY* has the highest percentage of visits, for both *SF1* and *SF2*, followed by *ADAPT\_S* and *ADAPT\_D*. This

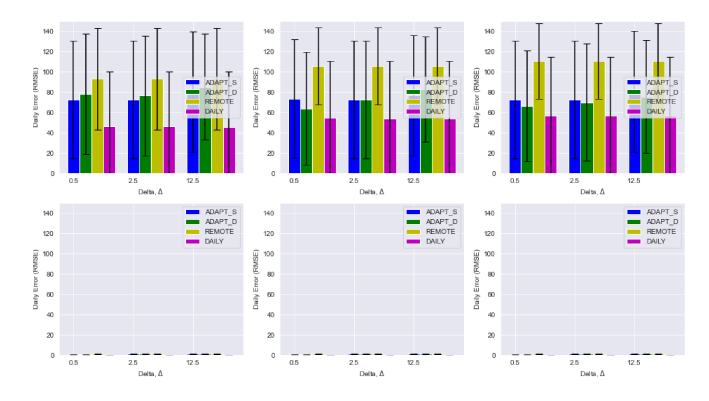


Fig. 4. Aggregated error (RMSE) in daily estimates of  $F_t \subset F$ , with  $Z_S$  acquiring data at 2 day (left), 5 day (center) and 10 day (right) intervals. Overall, DAILY (magenta) approach has the smallest error, closely followed by  $ADAPT\_S$  (blue) and  $ADAPT\_D$  (green), for both SFI (top row) and SF2 (bottom row). Remote (yellow) has the highest error across all scenarios.

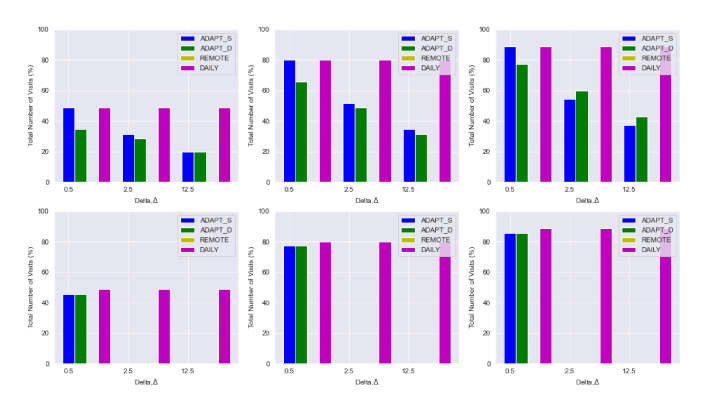


Fig. 5. Percentage of  $Z_G$  deployments based on each method across the time horizon, T, for cycles 2 days (left), 5 days (center), and 10 days (right). For both SF1 (top row) and SF2 (bottom row), DAILY (magenta) has the highest percentage of visits and REMOTE (yellow) has 0 across all cycles.  $ADAPT\_S$  (blue) reports the second highest percentage of deployments followed by  $ADAPT\_D$  (green).

high percentage of visits makes it impractical for implementing the DAILY strategy, especially in persistent environment monitoring, where technicians and domain experts need to be present on every monitoring mission. On the other hand, the relatively low visits when applying either ADAPT method is due to the implementation of the optimized deployment schedules. Moreover, when implementing either ADAPT strategy,  $Z_G$  visits less number of locations than under the DAILY strategy across all scenarios, as shown in Fig. 6. We also observe that  $Z_G$  visits less locations under  $ADAPT\_D$ than under ADAPT\_S. This indicates ADAPT\_D's ability to not only identify the right time to deploy  $Z_G$  but also select critical locations for sampling. This adaptive behavior is beneficial in minimizing the operational costs of  $Z_G$ . Overall, these advantages can be useful in optimizing sensor deployment schedules, thereby minimizing operational costs and logistical demands associated with running a persistent monitoring mission with portable sensors.

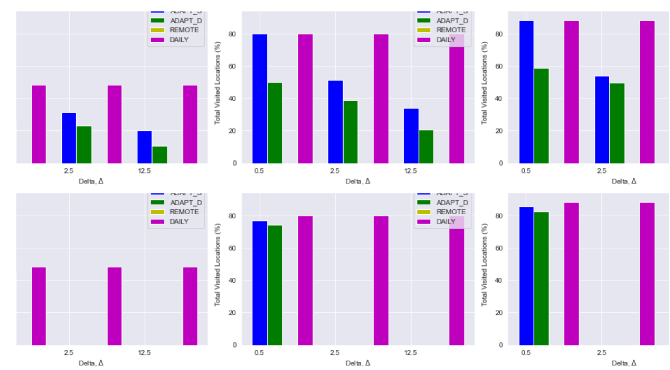


Fig. 6. Percentage of locations sampled by  $Z_G$  based on each method across the time horizon, T, for cycles 2 days (left), 5 days (center), and 10 days (right). Overall,  $Z_G$  samples the largest percentage of locations with the DAILY (magenta) strategy, followed by  $ADAPT\_S$  (blue) then  $ADAPT\_D$  (green) across all cycles, for both SFI (top row) and SF2 (bottom row). Note, the REMOTE (yellow) method will never deploy  $Z_G$ .

## VIII. CONCLUSIONS

We presented a decision-making framework that plans for when and where on-demand robot(s) should sample in an environment, based on previously collected data of past robotic deployments and remote sensing data. Analysis of temporal variance changes in a mixture of GP experts model estimates allows the decision-making framework to preserve a predictive accuracy over time, while minimizing the number of deployments. Our experiments with synthetic and real-world spatio-temporal phenomena demonstrated the effectiveness of our proposed approach compared to baseline strategies.

We plan to extend this work by determining how many and which types of robots, possibly equipped with different sensor quality tools, would be best to deploy. We expect to conduct a large scale experimental campaign over the summer to monitor cyanobacterial blooms in lakes.

Ultimately, our novel decision-making framework has the potential to significantly reduce the logistics and cost of data collection in the field, a vital requirement for operating various lake and ocean monitoring missions.

## ACKNOWLEDGEMENT

This work is supported in part by the Burke Research Initiation Award and NSF CNS-1919647, 2144624, OIA-1923004.

# REFERENCES

- M. Dunbabin and L. Marques, "Robots for environmental monitoring: Significant advancements and applications," *IEEE Robotics & Automation Magazine*, vol. 19, no. 1, pp. 24–39, 2012.
- [2] A. Erkkilä and R. Kalliola, "Patterns and dynamics of coastal waters in multi-temporal satellite images: Support to water quality monitoring in the archipelago sea, finland," *Estuarine, Coastal and Shelf Science*, vol. 60, no. 2, pp. 165–177, 2004.
- [3] Y. Huang, Y. Yao, J. Hansen, et al., "An autonomous probing system for collecting measurements at depth from small surface vehicles," OCEANS 2021: San Diego – Porto, 2021.
- [4] H. Cao, Z. Guo, S. Wang, H. Cheng, and C. Zhan, "Intelligent wide-area water quality monitoring and analysis system exploiting unmanned surface vehicles and ensemble learning," *Water*, vol. 12, no. 3, p. 681, 2020.

- [5] G. Ferri, A. Manzi, F. Fornai, F. Ciuchi, and C. Laschi, "The hydronet asv, a small-sized autonomous catamaran for real-time monitoring of water quality: From design to missions at sea," *IEEE Journal of Oceanic Engineering*, vol. 40, no. 3, pp. 710–726, 2014.
- [6] D. Karimanzira, M. Jacobi, T. Pfützenreuter, et al., "First testing of an auv mission planning and guidance system for water quality monitoring and fish behavior observation in net cage fish farming," Information Processing in Agriculture, vol. 1, no. 2, pp. 131–140, 2014
- [7] S. Bai, T. Shan, F. Chen, L. Liu, and B. Englot, "Information-driven path planning," *Current Robotics Reports*, pp. 1–12, 2021.
- [8] H. Choset and P. Pignon, "Coverage path planning: The boustrophedon cellular decomposition," in *Field and Service Robotics*, A. Zelinsky, Ed. London: Springer London, 1998, pp. 203–209.
- [9] A. Xu, C. Viriyasuthee, and I. Rekleitis, "Efficient complete coverage of a known arbitrary environment with applications to aerial operations," English, *Autonomous Robots*, vol. 36, no. 4, pp. 365–381, 2014
- [10] E. Galceran and M. Carreras, "A survey on coverage path planning for robotics," *Robotics and Autonomous systems*, vol. 61, no. 12, pp. 1258–1276, 2013.
- [11] M. Rahimi, R. Pon, W. J. Kaiser, G. S. Sukhatme, D. Estrin, and M. Srivastava, "Adaptive sampling for environmental robotics," in *IEEE International Conference on Robotics and Automation*, 2004. Proceedings. ICRA'04. 2004, IEEE, vol. 4, 2004, pp. 3537–3544.
- [12] P. F. Lermusiaux, T. Lolla, P. J. Haley Jr, et al., "Science of autonomy: Time-optimal path planning and adaptive sampling for swarms of ocean vehicles," Springer Handbook of Ocean Engineering, pp. 481–498, 2016.
- [13] J. L. Nguyen, N. R. Lawrance, R. Fitch, and S. Sukkarieh, "Real-time path planning for long-term information gathering with an aerial glider," *Autonomous Robots*, vol. 40, pp. 1017–1039, 2016.
- [14] S. Manjanna, A. Q. Li, R. N. Smith, I. Rekleitis, and G. Dudek, "Heterogeneous multi-robot system for exploration and strategic water sampling," in 2018 IEEE international conference on robotics and automation (ICRA), IEEE, 2018, pp. 4873–4880.
- [15] A. Quattrini Li, "Exploration and mapping with groups of robots: Recent trends," *Current Robotics Reports*, pp. 1–11, 2020.
- [16] V. Preston, G. Flaspohler, A. P. Michel, J. W. Fisher III, and N. Roy, "Robotic planning under uncertainty in spatiotemporal environments in expeditionary science," arXiv preprint arXiv:2206.01364, 2022.
- [17] M. Dunbabin and A. Grinham, "Quantifying spatiotemporal greenhouse gas emissions using autonomous surface vehicles," *Journal of field robotics*, vol. 34, no. 1, pp. 151–169, 2017.
- [18] J. Yu, M. Schwager, and D. Rus, "Correlated orienteering problem and its application to persistent monitoring tasks," *IEEE Transactions* on Robotics, vol. 32, no. 5, pp. 1106–1118, 2016.
- [19] R. N. Smith, M. Schwager, S. L. Smith, B. H. Jones, D. Rus, and G. S. Sukhatme, "Persistent ocean monitoring with underwater gliders: Adapting sampling resolution," *Journal of Field Robotics*, vol. 28, no. 5, pp. 714–741, 2011.
- [20] P. P. Neumann, S. Asadi, A. J. Lilienthal, M. Bartholmai, and J. H. Schiller, "Autonomous gas-sensitive microdrone: Wind vector estimation and gas distribution mapping," *IEEE robotics & automation magazine*, vol. 19, no. 1, pp. 50–61, 2012.
- [21] J. Binney, A. Krause, and G. S. Sukhatme, "Optimizing waypoints for monitoring spatiotemporal phenomena," *The International Journal of Robotics Research*, vol. 32, no. 8, pp. 873–888, 2013.
- [22] T. M. Sears and J. A. Marshall, "Mapping of spatiotemporal scalar fields by mobile robots using gaussian process regression," in 2022 IEEE/RSJ International Conference on Intelligent Robots and Systems (IROS), IEEE, 2022, pp. 6651–6656.
- [23] K.-C. Ma, Z. Ma, L. Liu, and G. S. Sukhatme, "Multi-robot informative and adaptive planning for persistent environmental monitoring," in *Distributed Autonomous Robotic Systems: The 13th International Symposium*, Springer, 2018, pp. 285–298.
- [24] T. O. Fossum, G. M. Fragoso, E. J. Davies, et al., "Toward adaptive robotic sampling of phytoplankton in the coastal ocean," Science Robotics, vol. 4, no. 27, eaav3041, 2019.
- [25] S. Garg and N. Ayanian, "Persistent monitoring of stochastic spatiotemporal phenomena with a small team of robots," arXiv preprint arXiv:1804.10544, 2018.
- [26] R. Marchant, F. Ramos, S. Sanner, et al., "Sequential bayesian optimisation for spatial-temporal monitoring," in UAI, Citeseer, 2014, pp. 553–562.

- [27] W. Chen and L. Liu, "Multi-objective and model-predictive tree search for spatiotemporal informative planning," in 2019 IEEE 58th Conference on Decision and Control (CDC), IEEE, 2019, pp. 5716– 5722.
- [28] J. A. Caley and G. A. Hollinger, "Data-driven comparison of spatiotemporal monitoring techniques," in OCEANS 2015-MTS/IEEE Washington, IEEE, 2015, pp. 1–7.
- [29] P. Morere, R. Marchant, and F. Ramos, "Sequential bayesian optimization as a pomdp for environment monitoring with uavs," in 2017 IEEE International Conference on Robotics and Automation (ICRA), IEEE, 2017, pp. 6381–6388.
- [30] J. M. Santos, T. Krajník, J. P. Fentanes, and T. Duckett, "Lifelong information-driven exploration to complete and refine 4-d spatiotemporal maps," *IEEE Robotics and Automation Letters*, vol. 1, no. 2, pp. 684–691, 2016.
- [31] Y-H. Kim and D. A. Shell, "Distributed robotic sampling of non-homogeneous spatio-temporal fields via recursive geometric subdivision," in 2014 IEEE International Conference on Robotics and Automation (ICRA), IEEE, 2014, pp. 557–562.
- [32] T. Salam, D. Kularatne, E. Forgoston, and M. A. Hsieh, "Adaptive sampling and energy efficient navigation in time-varying flows," in *Autonomous Underwater Vehicles*, Institution of Engineering and Technology, 2020, pp. 493–537.
- [33] R. Graham and J. Cortés, "A cooperative deployment strategy for optimal sampling in spatiotemporal estimation," in 2008 47th IEEE Conference on Decision and Control, IEEE, 2008, pp. 2432–2437.
- [34] K. Cheng, S. Chan, and J. H. Lee, "Remote sensing of coastal algal blooms using unmanned aerial vehicles (uavs)," *Marine Pollution Bulletin*, vol. 152, p. 110 889, 2020.
- [35] T. Salam and M. A. Hsieh, "Heterogeneous robot teams for modeling and prediction of multiscale environmental processes," arXiv preprint arXiv:2103.10383, 2022.
- [36] D. J. Lary, D. Schaefer, J. Waczak, et al., "Autonomous learning of new environments with a robotic team employing hyper-spectral remote sensing, comprehensive in-situ sensing and machine learning," Sensors, vol. 21, no. 6, p. 2240, 2021.
- [37] C. E. Rasmussen, "Gaussian processes in machine learning," in Summer school on machine learning, Springer, 2003, pp. 63–71.
- [38] H. Pishro-Nik, Introduction to probability, statistics, and random processes. QUBES Educational Resources, 2016.
- [39] V. Suryan and P. Tokekar, "Learning a spatial field in minimum time with a team of robots," *IEEE Transactions on Robotics*, vol. 36, no. 5, pp. 1562–1576, 2020.
- [40] S. Manjanna, A. Q. Li, R. N. Smith, I. Rekleitis, and G. Dudek, "Heterogeneous multi-robot system for exploration and strategic water sampling," in 2018 IEEE International Conference on Robotics and Automation (ICRA), 2018, pp. 4873–4880.
- [41] E. Schubert, J. Sander, M. Ester, H. P. Kriegel, and X. Xu, "Dbscan revisited, revisited: Why and how you should (still) use dbscan," ACM Transactions on Database Systems (TODS), vol. 42, no. 3, pp. 1–21, 2017.
- [42] M. Ester, H.-P. Kriegel, J. Sander, X. Xu, et al., "A density-based algorithm for discovering clusters in large spatial databases with noise," in kdd, vol. 96, 1996, pp. 226–231.
- [43] S. Chakraborty, N. K. Nagwani, and L. Dey, "Performance comparison of incremental k-means and incremental dbscan algorithms," arXiv preprint arXiv:1406.4751, 2014.
- [44] J. D. Little, K. G. Murty, D. W. Sweeney, and C. Karel, "An algorithm for the traveling salesman problem," *Operations research*, vol. 11, no. 6, pp. 972–989, 1963.
- [45] S. Müller, L. Schüler, A. Zech, and F. Heße, "GSTools v1.3: A toolbox for geostatistical modelling in python," *Geoscientific Model Development*, vol. 15, no. 7, pp. 3161–3182, 2022.
- [46] R. Vaughan, "Massively multi-robot simulation in stage," Swarm intelligence, vol. 2, no. 2, pp. 189–208, 2008.
- [47] A. E. Carter and C. T. Ragsdale, "A new approach to solving the multiple traveling salesperson problem using genetic algorithms," *European journal of operational research*, vol. 175, no. 1, pp. 246– 257, 2006.